AGU PUBLICATIONS

Geophysical Research Letters

RESEARCH LETTER
10.1002/2014GL059515

Key Points:
- To better predict the ion escape rate from Martian upper atmosphere
- To understand the long-term evolution of Mars atmosphere over its history
- To support MAVEN spacecraft mission planning and data analysis (2013–2016)

Correspondence to:
C. Dong,
dcfy@umich.edu

Citation:
Dong, C., S. W. Bougher, Y. Ma, G. Toth, A. F. Nagy, and D. Najib (2014), Solar wind interaction with Mars upper atmosphere: Results from the one-way coupling between the multifluid MHD model and the MTGCM model, *Geophys. Res. Lett.*, *41*, 2708–2715, doi:10.1002/2014GL059515.

Received 6 FEB 2014
Accepted 2 APR 2014
Accepted article online 3 APR 2014
Published online 23 APR 2014

Solar wind interaction with Mars upper atmosphere: Results from the one-way coupling between the multifluid MHD model and the MTGCM model

Chuanfei Dong[1], Stephen W. Bougher[1], Yingjuan Ma[2], Gabor Toth[1], Andrew F. Nagy[1], and Dalal Najib[3]

[1]Department of Atmospheric, Oceanic and Space Sciences, University of Michigan, Ann Arbor, Michigan, USA, [2]Department of Earth and Space Sciences, University of California, Los Angeles, California, USA, [3]National Academy of Sciences, Washington, District of Columbia, USA

Abstract The 3-D multifluid Block Adaptive Tree Solar-wind Roe Upwind Scheme (BATS-R-US) MHD code (MF-MHD) is coupled with the 3-D Mars Thermospheric general circulation model (MTGCM). The ion escape rate from the Martian upper atmosphere is investigated by using a one-way coupling approach, i.e., the MF-MHD model incorporates the effects of 3-D neutral atmosphere profiles from the MTGCM model. The calculations are carried out for two cases with different solar cycle conditions. The calculated total ion escape flux (the sum of three major ionospheric species, O^+, O_2^+, and CO_2^+) for solar cycle maximum conditions (6.6×10^{24} s^{-1}) is about 2.6 times larger than that of solar cycle minimum conditions (2.5×10^{24} s^{-1}). Our simulation results show good agreement with recent observations of 2–3 $\times 10^{24}$ s^{-1} (O^+, O_2^+, and CO_2^+) measured near solar cycle minimum conditions by Mars Express. An extremely high solar wind condition is also simulated which may mimic the condition of coronal mass ejections or corotating interaction regions passing Mars. Simulation results show that it can lead to a significant value of the escape flux as large as 4.3×10^{25} s^{-1}.

1. Introduction

The Sun has a powerful influence on planetary atmospheres. This is especially true for planets lacking a global intrinsic magnetic field, because the solar wind can interact directly with the upper atmosphere. Mars has no dipole magnetic field; instead, it has a crustal magnetic field [*Acuña et al.*, 1999], which makes the solar wind interaction with Martian upper atmosphere very complicated and unique. The crustal field is mainly concentrated in the Southern Hemisphere where it is highly localized. The strongest crustal sources exist at latitudes poleward of 30°S and at longitudes between 120°W and 210°W.

Recently, *Lundin et al.* [2008] found that the new energy settings introduced in May 2007 enabled the Mars Express (MEX) Analyzer of Space Plasma and Energetic Atoms (ASPERA-3) ion mass analyzer to accurately cover the low-energy range (10–100 eV) for all ions, especially the cold ionospheric ions. Measurements with these new settings reveal in great detail the low-energy comet-like ion outflow, inferred from Phobos-2. They found that the low-energy coverage greatly increased the observed Mars ion escape rates to more than $\sim 10^{25}$ ions/s during the solar cycle maximum conditions.

The study of the solar wind interaction with Mars upper atmosphere/ionosphere has received a great deal of attention during the last decade. Among the large number of topics in this research area, the investigation of ion escape fluxes has become increasingly important due to its potential impact on the long-term evolution of Mars atmosphere (e.g., loss of water) over its history. A number of papers reporting on the measurement of escape fluxes by the ASPERA-3 instrument on the Mars Express spacecraft have been published [e.g., *Lundin et al.*, 2008; *Barabash et al.*, 2007; *Nilsson et al.*, 2011]. Ion escape rates calculated by different plasma models, i.e., multispecies MHD model [*Ma et al.*, 2004; *Ma and Nagy*, 2007], test particle model [*Fang et al.*, 2010; *Curry et al.*, 2013], multifluid MHD model [*Harnett and Winglee*, 2006; *Najib et al.*, 2011; *Riousset et al.*, 2013], and hybrid model [*Modolo et al.*, 2006; *Brecht and Ledvina*, 2012] have also been published. These multidimensional plasma codes are all actively participating in an ongoing International Space Studies Institute effort focused upon the intercomparison of global models and measurements of the Martian plasma environment [*Brain et al.*, 2010]. However, all of these works are based on 1-D spherically symmetric neutral atmosphere profiles except the work by *Ma and Nagy* [2007] which incorporates the effect

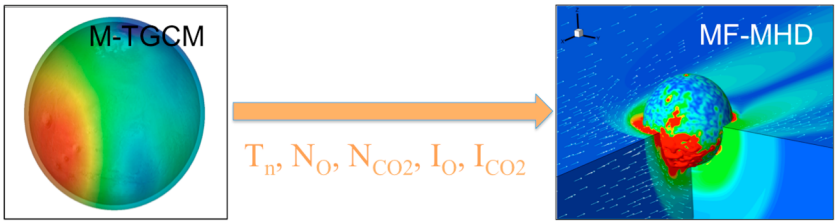

Figure 1. A sketch (cartoon) of a one-way coupling approach between MTGCM and MF-MHD models. The notation T_n denotes neutral atmosphere temperatures, N_O, N_{CO_2} are the neutral O and CO_2 number densities, and I_O, I_{CO_2} are the photoionization frequencies.

of 3-D neutral profiles from the existing MTGCM model developed by *Bougher et al.* [2000, 2006, 2009]. The multispecies MHD model, however, solves only one momentum and one energy equation for all different ion species; therefore, it cannot capture the dynamics of individual ion species.

In the present work, we adopt the 3-D Mars neutral atmosphere profiles (i.e., neutral atmosphere temperatures T_n, neutral densities N_O, N_{CO_2}, and photoionization frequencies I_O, I_{CO_2} as shown in Figure 1) from the MTGCM model and one-way couple it with the MF-MHD model that solves separate momentum and energy equations for each ion species [*Powell et al.*, 1999; *Glocer et al.*, 2009; *Najib et al.*, 2011; *Tóth et al.*, 2012]. We also compare the simulation results with the currently available observational data. Meanwhile, this work has the potential to provide predictions of ion escape rates for comparison to future data to be returned by the Mars Atmosphere and Volatile EvolutioN (MAVEN) mission (2013–2016).

2. Model Description

The MTGCM model is a finite difference primitive equation model that self-consistently solves for time-dependent neutral temperatures, neutral-ion densities, and three-component neutral winds over the Mars globe [e.g., *Bougher et al.*, 2000, 2006, 2008, 2009]. The modern MTGCM code contains prognostic equations for the major neutral species (CO_2, CO, N_2, and O), selected minor neutral species (Ar, NO, N(^4S), and O_2), and several photochemically produced ions (O_2^+, CO_2^+, O^+, CO^+, and NO^+). The resolutions in latitude and longitude are 5°. The vertical coordinate is log pressure with a resolution equaling to 0.5 scale heights (which is about 5 km in the Martian lower thermosphere). All fields are calculated on 33 pressure levels above 1.32 μbar, corresponding to altitudes from roughly 70 to 300 km (at solar maximum conditions). The MTGCM model is thermally and dynamically coupled with the NASA Ames Mars general circulation model (5° × 5° grid) [*McDunn et al.*, 2010]. The $E_{10.7}$ or $F_{10.7}$ cm index (solar EUV/UV flux variation), the heliocentric distance, and the solar declination corresponding to Mars seasons are the key adjustable parameters in the model that can be varied for investigating different MTGCM cases. A fast nonlocal thermodynamic equilibrium 15 μm cooling scheme is implemented in the MTGCM, dynamically dependent upon simulated atomic O abundances, along with corresponding near-IR heating rates *Bougher et al.* [2006]. The model is constrained by observations from MGS (Mars Global Surveyor), Mars Odyssey, and Mars Reconnaissance Orbiter [see *Bougher et al.*, 2008].

In order to one-way couple the MTGCM model with the MF-MHD model, we initialize the latter (from 100 km to 5 R_M, where R_M is the radius of Mars ~ 3396 km) with the 3-D neutral profiles (i.e., T_n, N_O, N_{CO_2}, I_O, and I_{CO_2}). The equinox season (solar longitude = 180°) for both solar minimum ($F_{10.7}$ = 70) and solar maximum ($F_{10.7}$ = 200) conditions is considered. Since both models are built on spherical coordinates, we can linearly interpolate the cell value from one to the other in the overlapping domains of each model (100 km to 250 km). From 250 km to 5 R_M, we assume constant neutral temperature and photoionization frequencies based on the MTGCM upper boundary values since these values are almost constant when approaching the MTGCM outer boundary. For the neutral atmosphere densities, however, we use an extrapolation based upon the hydrostatic assumption which assumes the neutral atmosphere densities decrease exponentially with altitude, i.e., $n = n_0 \exp(-dz/H)$, where dz is the altitude change and H is the scale height (which depends on the gravity, neutral temperature, and neutral species mass). The hot atom densities are taken from *Kim et al.* [1998] that are assumed to be spherically symmetric. We also adopted more realistic collision frequencies between species [*Schunk and Nagy*, 2009]. In order to make the code run more efficiently, we use large super cells in the polar regions [*Tóth et al.*, 2012], which can accelerate the speed of model

Table 1. Input Parameters Used for the Different Calculations

Simulation Cases	Solar Condition	Solar Wind Density (cm^{-3})	Upstream B Field	Solar Wind Velocity (km/s)	Subsolar Position[a]
Case 1	Solar Minimum	4	3 nT Parker Spiral	400	180°W 0°N
Case 2	Solar Maximum	4	3 nT Parker Spiral	400	180°W 0°N
Case 3	Solar Maximum	20	B_y=20 nT, B_x=B_z=0	1000	180°W 0°N

[a]The crustal fields face the Sun.

convergence, and allow larger time steps for time accurate simulations. This new grid structure will enable us to investigate the effects of some dynamic events (such as coronal mass ejections (CMEs) and Martian dust storm) on the ion escape flux in the future. Unless mentioned otherwise, the other parameters are the same as those in *Najib et al.* [2011].

The MF-MHD model was described in detail in the previous paper [*Najib et al.*, 2011], thus we only briefly summarize the model here. The newly developed 3-D MF-MHD [*Najib et al.*, 2011] can better simulate the interplay between Martian upper atmosphere and solar wind by considering the dynamics of individual ion species. In the multifluid formulation, we have separate continuity, momentum, and energy equations for the four ion fluids H^+, O^+, O_2^+, and CO_2^+. The lower boundary is set at 100 km above the Martian surface, where the O^+, O_2^+, and CO_2^+ densities are taken to be the photochemical equilibrium values. Given the solar wind proton can penetrate into the ionosphere to some extent, the H^+ density at the inner boundary is set to be approximately 30% of the solar wind density, $0.3N_{sw}$. The model adopts a nonuniform, spherical grid structure with a radial resolution varying from 5 km at the lower boundary to 1000 km at the outer boundary ($\sim$ 20 Mars radii) and with angular resolution varying from 1.5° to 3°. We choose the smallest vertical resolution as 5 km since we want to capture all the vertical structure of the neutral profiles from the MTGCM model. The x axis in the coordinate system points from Mars toward the Sun, the rotation axis is in the x-z plane, and the y axis completes the right-hand system. The computational domain is defined by $-24\ R_M \le X \le 8\ R_M$; $-16\ R_M \le Y, Z \le 16\ R_M$. A reflective inner boundary condition for the velocity $\mathbf{u}$ is used, which results in near-zero velocity at the inner boundary as expected. The plasma temperature, $T_p = T_i + T_e$, at the inner boundary is set to be twice the value of the neutral temperature, T_n, because at that low altitude, both ions (T_i) and electrons (T_e) have roughly the same temperature as neutrals.

The upstream solar wind plasma temperatures are set to 3.5×10^5 K, and the interplanetary magnetic field (IMF) is assumed to be a Parker spiral in the X-Y plane with an angle of 56° for the first two cases. We use the 60° harmonic expansion for the crustal magnetic field developed by *Arkani-Hamed* [2001] to describe the observed fields at Mars [*Acuña et al.*, 1999]. The chemical reaction calculations include charge exchange, photoionization, and electron impact ionization; in order to calculate the latter, the model assumes that the electron temperature is half of the calculated plasma temperature and uses the ionization rates given by *Cravens et al.* [1987]. We adopt the same chemical reaction schemes as *Ma et al.* [2004] and *Ma and Nagy* [2007] in order to allow direct comparison with the multispecies model results.

3. Simulation Results and Discussions

In order to evaluate the effects of different solar radiation, interplanetary field magnitudes, solar wind density, and velocity on the Mars upper atmosphere ion escape fluxes, we first study two standard cases for solar minimum and solar maximum conditions. A case for solar maximum conditions with extremely high solar wind parameters (i.e., high solar wind velocity, strong upstream magnetic field, and large solar wind density) is also investigated to estimate the level of the enhanced ion escape flux for such an extreme environment. Table 1 summarizes the parameters used for the three different cases.

Compared with the multispecies MHD model [*Ma et al.*, 2004], the multifluid MHD model employs separate mass, momentum, and energy equations for the four ion fluids [*Najib et al.*, 2011]. The differences caused by solving individual momentum and energy equations for different ion species are shown in Figure 2, where the main feature is the asymmetric escape plume shape for heavy ion species. The asymmetry is primarily caused by different Lorentz forces acting on each ion species. In the individual ion momentum equations, the MF-MHD model includes the Lorentz force $n_s q_s(\mathbf{u_s} \times \mathbf{B} + \mathbf{E})$:

$$\frac{\partial \rho_s \mathbf{u_s}}{\partial t} + \nabla \cdot \left(\rho_s \mathbf{u_s}\mathbf{u_s} + Ip_s\right) = n_s q_s(\mathbf{u_s} \times \mathbf{B} + \mathbf{E}) + S_{\rho_s u_s} \quad (1)$$

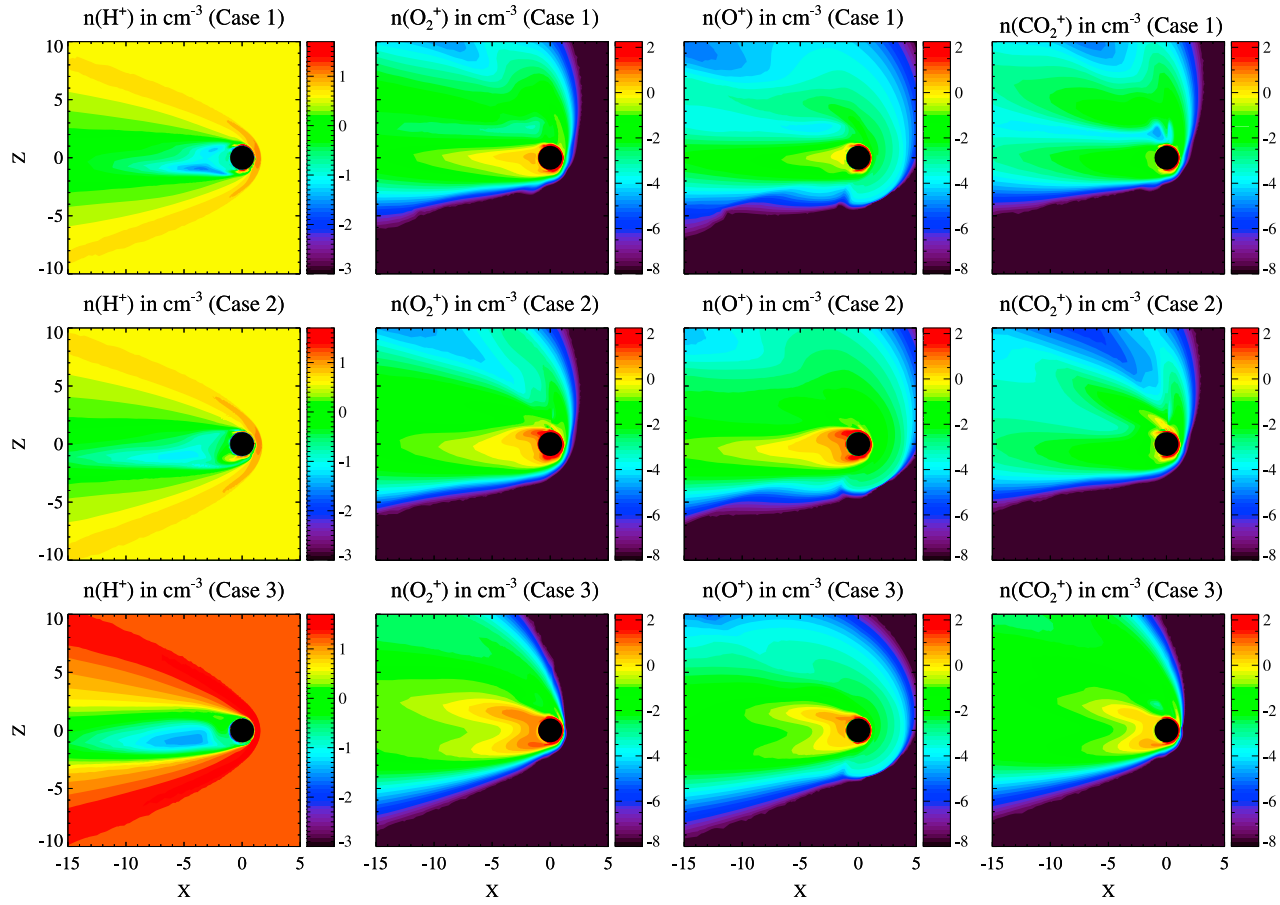

Figure 2. The calculated ion number densities in cm^{-3} in the *X-Z* plane for H^+, O_2^+, O^+, and CO_2^+ in a logarithmic scale. Note that the logarithmic scales in different plots are different.

where ρ_s, n_s, q_s, $\mathbf{u_s}$, and p_s are the individual mass density, number density, charge, velocity, and pressure of the ion species *s*, respectively. $\mathbf{E}$ and $\mathbf{B}$ denote the electric and magnetic fields, $\mathbf{J}$ is the current density, *I* is the identity matrix, *e* is the electric charge, and $S_{\rho_s u_s}$ is the momentum source term. The electric field $\mathbf{E}$ can be calculated from the generalized Ohm's law:

$$\mathbf{E} = -\frac{\nabla p_e}{en_e} - \mathbf{u_e} \times \mathbf{B} = -\frac{\nabla p_e}{en_e} - \left(\mathbf{u}_+ - \frac{\mathbf{J}}{en_e}\right) \times \mathbf{B} \tag{2}$$

where $\mathbf{u_e}$ and $\mathbf{u}_+ = \sum_s n_s q_s \mathbf{u_s}/(en_e)$ are the electron fluid velocity and the charge averaged ion velocity, respectively. The electron pressure is denoted by p_e and the term $\mathbf{J} \times \mathbf{B}/(en_e)$ on the right-hand side is called the *Hall term*. Substituting $\mathbf{E}$ into the ion momentum equation, we are left with

$$\frac{\partial \rho_s \mathbf{u_s}}{\partial t} + \nabla \cdot (\rho_s \mathbf{u_s} \mathbf{u_s} + Ip_s) = n_s q_s (\mathbf{u_s} - \mathbf{u}_+) \times \mathbf{B} + \frac{n_s q_s}{n_e e}(\mathbf{J} \times \mathbf{B} - \nabla p_e) + S_{\rho_s u_s} \tag{3}$$

It can easily be proved that $(\mathbf{u_s} - \mathbf{u}_+) \times \mathbf{B}$ term will lead to a flow asymmetry in the *X-Z* plane only, as long as the magnetic field is in the *X-Y* plane. Thus, the plume provides a channel for ions to escape while this cannot be captured by the multispecies model. Given all the ion species are fully picked up by the solar wind eventually and ignoring the friction resulted from the source term, the characteristic spatial scale, L_g, associated with the asymmetry is controlled by the ratio $m_s u_{sw}/(q_s B)$ via dimensional analysis. Actually, L_g is the characteristic spatial scale for the heavy ion fluid to reach the solar wind speed, u_{sw}, or to be fully picked up. Therefore, the heavier the ions are (note $q_s = e$ in the model), the more significant the escape plume is. On the other hand, from the particle simulation point of view, the asymmetry can also be explained by the induced electric field [*Fang et al.*, 2010].

Table 2. Calculated Ion Escape Fluxes (in s^{-1})

MHD Model	Neutral Profile	Simulation Cases	O^+	O_2^+	CO_2^+	Total
Multifluid	3-D MTGCM	Case 1	4.2×10^{23}	1.7×10^{24}	3.5×10^{23}	2.5×10^{24}
		Case 2	3.7×10^{24}	2.5×10^{24}	3.8×10^{23}	6.6×10^{24}
		Case 3	1.0×10^{25}	2.5×10^{25}	8.2×10^{24}	4.3×10^{25}
Multifluid[a]	1-D	Case 2	7.7×10^{23}	9.0×10^{23}	1.7×10^{23}	1.84×10^{24}
Multispecies[b]	3-D MTGCM	Case 1	7.2×10^{23}	1.9×10^{23}	1.3×10^{23}	1.0×10^{24}
		Case 2	1.8×10^{24}	4.1×10^{23}	1.8×10^{23}	2.4×10^{24}
		Case 3	2.3×10^{25}	3.3×10^{24}	4.1×10^{24}	3.0×10^{25}

[a]The case 2 shows the results from *Najib et al.* [2011] by adopting the 1-D spherically symmetric neutral atmosphere, where they defined the case 2 we studied here as case 4.

[b]The multispecies simulation results are from *Ma and Nagy* [2007], where they labeled the cases 1, 2, and 3 we studied here as their cases 4, 6, and 7.

Comparing case 1 with case 2 (see Figure 2), the ion escape plume is more significant for the solar maximum conditions and the density close to the planet is increased. This is caused by the enhanced solar radiation during the solar maximum conditions which increases the amount of ions. Therefore, the ion escape rate for case 2 should be larger than that of case 1. Case 3 is motivated by Pioneer Venus observations which measured very high escaping ion fluxes from Venus during significantly increased solar wind pressure conditions [*Luhmann et al.*, 2007]. Thus, the simulation results of case 3 may yield an estimation of ionospheric outflow during some extreme conditions such as CMEs and corotating interaction regions (CIRs). Inspection of Figure 2 reveals that the asymmetry in case 3 becomes less obvious than case 1 and case 2 while the escape plumes in the regions near Mars body become even stronger compared with case 2. This is because the characteristic spatial scale, L_g, associated with the asymmetry is controlled by the ratio $m_s u_{sw}/(q_s B)$.

We summarize the calculated ion escape fluxes by adopting different MHD models and neutral atmosphere profiles in Table 2. The calculation is conducted by integrals of the plasma density times the radial velocity component at the surface of a sphere far from the planet. In this paper, we select the integral spherical surface to be 6 R_M since we find that the calculated ion escape fluxes do not change to any significant degree once the radius exceeds 4 R_M. *Lundin et al.* [2008] suggested that the total ion escape rate (O^+, O_2^+, and CO_2^+) is around 3×10^{24} s^{-1} during solar cycle minimum conditions and it may achieve values more than 10^{25} s^{-1} during solar cycle maximum conditions. *Nilsson et al.* [2011] found that the net ion escape flux for solar cycle minimum conditions is around 2×10^{24} s^{-1}. Our total ion escape flux for solar minimum conditions (case 1) is 2.5×10^{24} s^{-1}, which is reasonably consistent with the available MEX observations. It is of particular interest to find that the calculated total ion escape flux for solar maximum conditions is about 2.6 times larger than that of solar minimum conditions, which is in good agreement with the value (~ 2.5) suggested by *Verigin et al.* [1991] and *Nilsson et al.* [2011]. As we expected from Figure 2, the total ion escape flux for extreme case (case 3) is 1 order of magnitude larger than case 1 and case 2, and the value is on the order of 10^{25} s^{-1} which is again consistent with the value suggested by *Lundin et al.* [2008].

Compared with the multispecies MHD simulation results (Table 2), the MF-MHD calculations show that the O^+ escape flux generally becomes smaller while the O_2^+, CO_2^+, and total escape fluxes increase for all three cases. One of the main reasons is that the heavy ions have a significant asymmetric ion escape plume, and therefore, the MF-MHD code provides a new channel for ions to escape; this feature, however, cannot be captured by the multispecies MHD model. On the other hand, the escape flux also greatly depends on the ionospheric chemical reactions in the model (refer to *Najib et al.* [2011, Table 1]), e.g., CO_2^+ is produced only from photoionization while it is consumed by three chemical reactions, indicating the CO_2^+ escape flux is less than that of O_2^+. In addition, the MTGCM code has been improved since its output was first utilized in the multispecies MHD model of *Ma and Nagy* [2007]. Recent MTGCM improvements include the following: (a) updated lower atmosphere forcing using dust opacity distributions from the MGS/Thermal Emission Spectrometer [*Smith*, 2004] and (b) the adoption of new solar fluxes (1.0 nm bins) from the empirically based Flare Irradiance Spectral Model of *Chamberlin et al.* [2008] for solar minimum and maximum conditions. Given the different model setup and input, we cannot compare quantitatively our simulation results with the previous similar case studies [see, e.g., *Harnett and Winglee*, 2006; *Brecht and Ledvina*, 2012]. However, it is interesting to mention that both models [*Harnett and Winglee*, 2006; *Brecht and Ledvina*, 2012] show that O_2^+ is dominant over other heavy ion species during the ion escape, which is reasonably consistent with our

simulation results. Their simulation results also indicate that the dayside crustal field has a shielding effect that tends to reduce the ion escape flux in the process of ion loss, which is consistent with the results shown by *Ma et al.* [2004].

In general, for the MF-MHD simulation, all the ion escape fluxes increase for the 3-D neutral input compared with the 1-D case (see Table 2). The 3-D neutral atmosphere basically changes the atmosphere temperature T_n, densities, and the photoionization frequencies of neutral species O and CO_2 compared to the previous studies [*Najib et al.*, 2011]. In the 3-D neutral upper atmosphere, the major Martian atmosphere components (CO_2 and O) are no longer symmetric about the planet. There exists more neutral CO_2 on the dayside than nightside (at a constant altitude) because the CO_2 global distribution is mainly controlled by the temperature structure and not the dynamics. The neutral CO_2 densities are enhanced (reduced) on the dayside (nightside) where temperatures are warmer (colder). Neutral O, however, is mainly controlled by transport due to its relatively small mass. The neutral wind will transport neutral O from dayside to nightside, resulting in a bulge of neutral O in the nightside upper atmosphere. Hence, it is more realistic to use the 3-D atmospheric structure from the MTGCM model than the 1-D neutral atmosphere. The significant change in (MHD) model input indicates that the MTGCM neutral profiles essentially increase the ion sources resulting from various ionization processes (i.e., photoionization, charge exchange, and electron impact ionization), which in turn enhances the ion escape flux. It is noteworthy that although the MTGCM model provides the MF-MHD code with 3-D neutral atmosphere profiles that are certainly more realistic (i.e., asymmetric about the globe), there are presently no accurate measurements of the (thermal and suprathermal) oxygen profiles in the Mars atmosphere [*Bougher et al.*, 2008]. This uncertainty will affect the calculated ion escape fluxes. Therefore, the neutral atmosphere profiles to be returned by the MAVEN mission will significantly reduce the uncertainty in calculated escape rates resulting from the lack of direct information regarding the oxygen abundance.

Besides providing better input to models, MAVEN also has the opportunity to test specific predictions from the models. For instance, MAVEN could test the enhanced ion escape fluxes during various extreme events, such as CMEs/CIRs/solar energetic particles and Martian dust storms and compare them with simulation results, which could help to improve the models with the possible missing physics. It is also possible that MAVEN could make direct observations of the magnetic reconnection in the near Martian magnetotail by its magnetometer, as has been observed near Venus by Venus Express [*Zhang et al.*, 2012]. To better study the magnetotail reconnection, one has to adopt adaptive mesh refinement to refine the blocks in the magnetotail region in order to reduce the numerical diffusion. Meanwhile, one needs to employ the resistive MHD model, where the electrical conductivity, σ, is no longer infinite. Although the heavy ion (such as O^+) cyclotron waves generated from the pickup of exospheric O^+ have never been observed, they may be an important source for heating the cold ionospheric O^+ [*Dong et al.*, 2013]. MAVEN may be able to investigate the existence of these waves upstream of the Martian bow shock using the Langmuir probe and waves antenna. In order to investigate this problem, high-resolution global hybrid simulations are essential. In short, the scientific return from the MAVEN mission will benefit greatly from combining its future returned data with various model results.

4. Conclusions

In summary, we studied the solar wind interaction with Martian upper atmosphere by using a one-way coupling of two comprehensive 3-D models, i.e., the MTGCM thermosphere-ionosphere model output is used as input for the MF-MHD model. Our model predicted ion escape fluxes are in good agreement with the recent observational data. The immediate impact of the work will be improvements to estimated ion escape fluxes and global ion escape rates. Furthermore, this work has the potential to provide improved predictions of ion escape rates for comparison to future data to be returned by the MAVEN mission (2013–2016) and thereby improve our understanding of the present-day escape processes.

Additionally, we plan to further investigate the solar wind interaction with the Martian upper atmosphere using a more sophisticated coupling approach. In future work, we will adopt the 3-D Mars cold neutral atmosphere profiles (100–300 km) from the newly developed and validated ground to exosphere Mars Global Ionosphere Thermosphere Model (MGITM) [*Bougher et al.*, 2011] and the 3-D hot oxygen profiles (100 km to 5 R_M) from the Direct Simulation Monte Carlo (DSMC) Exosphere Model [*Valeille et al.*, 2009]. We will exchange these 3-D model output fields with the 3-D BATS-R-US Mars multifluid MHD model

(100 km to 20 R_M). The MGITM model together with the DSMC model take into account the effects of solar cycle and seasonal variations on both cold and hot neutral atmospheres. This will allow us to investigate the corresponding effects on the Martian upper atmosphere ion escape by using a one-way coupling approach (i.e., both the MGITM and DSMC model output will be used as input for the MF-MHD model). Moreover, one-way coupling is a necessary precursor to future full two-way integration of various models since the two-way integration requires using a combination of MF-MHD, MGITM, and DSMC codes to solve for the overlapping domains of each model (100–300 km).

Acknowledgments
The work was partially supported by NASA Earth and Space Science Fellowship NNX13AO56H and NASA grant NNH10CC04C. C.F. Dong wants to acknowledge the Vela fellowship support from LANL. We would like to acknowledge high-performance computing support from Yellowstone (ark:/85065/d7wd3xhc) provided by NCAR's Computational and Information Systems Laboratory (CISL), sponsored by the National Science Foundation. The data for this paper are available at Yellowstone (supercomputer) provided by NCAR's CISL (path: /glade/p/work/).

The Editor thanks Thomas Cravens and an anonymous reviewer for their assistance in evaluating this paper.

References

Acuña, M. H., et al. (1999), Global distribution of crustal magnetization discovered by the Mars global surveyor MAG/ER experiment, *Science*, *284*, 790–793.

Arkani-Hamed, J. (2001), A 50-degree spherical harmonic model of the magnetic field of Mars, *J. Geophys. Res.*, *106*, 23,197–23,208.

Barabash, S., A. Fedorov, R. Lundin, and J. A. Sauvaud (2007), Martian atmospheric erosion rates, *Science*, *315*, 501–503.

Bougher, S. W., S. Engel, R. G. Roble, and B. Foster (2000), Comparative terrestrial planet thermospheres 3. Solar cycle variation of global structure and winds at solstices, *J. Geophys. Res.*, *105*, 17,669–17,692.

Bougher, S. W., J. M. Bell, J. R. Murphy, M. A. Lopez-Valverde, and P. G. Withers (2006), Polar warming in the Mars thermosphere: Seasonal variations owing to changing insolation and dust distributions, *Geophys. Res. Lett.*, *33*, L02203, doi:10.1029/2005GL024059.

Bougher, S. W., P.-L. Blelly, M. R. Combi, J. L. Fox, I. Mueller-Wodarg, A. Ridley, and R. G. Roble (2008), Neutral upper atmosphere and ionosphere modeling, *Space Sci. Rev.*, *139*, 107–141.

Bougher, S. W., T. M. McDunn, K. A. Zoldak, and J. M. Forbes (2009), Solar cycle variability of Mars dayside exospheric temperatures: Model evaluation of underlying thermal balances, *Geophys. Res. Lett.*, *36*, L05201, doi:10.1029/2008GL036376.

Bougher, S. W., A. Ridley, D. Pawlowski, J. M. Bell, and S. Nelli (2011), Development and validation of the Ground-to-Exosphere Mars GITM Code: Solar cycle and seasonal variations of the upper atmosphere, in *Fourth International Workshop on the Mars Atmosphere: Modeling and Observations*, edited by F. Forget and E. Millour, pp. 379–381, NASA, Paris, France.

Brain, D., et al. (2010), A comparison of global models for the solar wind interaction with Mars, *Icarus*, *206*, 139–151.

Brecht, S. H., and S. A. Ledvina (2012), Control of ion loss from Mars during solar minimum, *Earth Planets Space*, *64*, 165–178.

Chamberlin, P. C., T. N. Woods, and F. G. Eparvier (2008), Flare Irradiance Spectral Model (FISM): Flare component algorithms and results, *Space Weather*, *6*, S05001, doi:10.1029/2007SW000372.

Cravens, T. E., J. U. Kozyra, A. F. Nagy, T. I. Gombosi, and M. Kurtz (1987), Electron impact ionization in the vicinity of comets, *J. Geophys. Res.*, *92*, 7341–7353.

Curry, S. M., M. W. Liemohn, X.-H. Fang, Y.-J. Ma, and J. Espley (2013), The influence of production mechanisms on pick-up ion loss at Mars, *J. Geophys. Res. Space Physics*, *118*, 554–569, doi:10.1029/2012JA017665.

Dong, C. F., M. M. Cowee, and D. Winske (2013), Plasma and wave properties downstream of Martian bow shock: Hybrid simulations, in *2013 Los Alamos Space Weather Summer School Research Reports*, edited by J. Koller and R. D. Gurule, pp. 11–18, Los Alamos National Lab, N. M.

Fang, X., M. W. Liemohn, A. F. Nagy, J. G. Luhmann, and Y. J. Ma (2010), On the effect of the Martian crustal magnetic field on atmospheric erosion, *Icarus*, *206*, 130–138.

Glocer, A., G. Tóth, Y. J. Ma, T. I. Gombosi, J. C. Zhang, and L. M. Kistler (2009), Multifluid Block-Adaptive-Tree Solar wind Roe-Type Upwind Scheme: Magnetospheric composition and dynamics during geomagnetic storms—Initial results, *J. Geophys. Res.*, *114*, A12203, doi:10.1029/2009JA014418.

Harnett, E. M., and R. M. Winglee (2006), Three-dimensional multifluid simulations of ionospheric loss at Mars from nominal solar wind conditions to magnetic cloud events, *J. Geophys. Res.*, *111*, A09213, doi:10.1029/2006JA011724.

Kim, J., A. F. Nagy, J. L. Fox, and T. E. Cravens (1998), Solar cycle variability of hot oxygen atoms at Mars, *J. Geophys. Res.*, *103*(A12), 29,339–29,342, doi:10.1029/98JA02727.

Luhmann, J. G., W. T. Kasprzak, and C. T. Russell (2007), Space weather at Venus and its potential consequences for atmosphere evolution, *J. Geophys. Res.*, *112*, E04S10, doi:10.1029/2006JE002820.

Lundin, R., S. Barabash, M. Holmström, H. Nilsson, M. Yamauchi, M. Fraenz, and E. M. Dubinin (2008), A comet-like escape of ionospheric plasma from Mars, *Geophys. Res. Lett.*, *35*, L18203, doi:10.1029/2008GL034811.

Ma, Y. J., A. F. Nagy, I. V. Sokolov, and K. C. Hansen (2004), Three-dimensional, multispecies, high spatial resolution MHD studies of the solar wind interaction with Mars, *J. Geophys. Res.*, *109*, A07211, doi:10.1029/2003JA010367.

Ma, Y. J., and A. F. Nagy (2007), Ion escape fluxes from Mars, *Geophys. Res. Lett.*, *34*, L08201, doi:10.1029/2006GL029208.

McDunn, T. L., S. W. Bougher, J. Murphy, M. D. Smith, F. Forget, J.-L. Bertaux, and F. Montmessin (2010), Simulating the density and thermal structure of the middle atmosphere (80–130 km) of Mars using the MGCM-MTGCM: A comparison with MEX/SPICAM observations, *Icarus*, *206*, 5–17.

Modolo, R., G. M. Chanteur, E. Dubinin, and A. P. Matthews (2006), Simulated solar wind plasma interaction with the Martian exosphere: Influence of the solar EUV flux on the bow shock and the magnetic pile-up boundary, *Ann. Geophys.*, *24*, 3403–3410.

Najib, D., A. F. Nagy, G. Tóth, and Y. J. Ma (2011), Three-dimensional, multifluid, high spatial resolution MHD model studies of the solar wind interaction with Mars, *J. Geophys. Res.*, *116*, A05204, doi:10.1029/2010JA016272.

Nilsson, H., N. J. Edberg, G. Stenberg, S. Barabash, M. Holmström, Y. Futaana, R. Lundin, and A. Fedorov (2011), Heavy ion escape from Mars, influence from solar wind conditions and crustal magnetic fields, *Icarus*, *215*, 475–484.

Powell, K. G., P. L. Roe, T. J. Linde, T. I. Gombosi, and D. L. De Zeeuw (1999), A solution-adaptive upwind scheme for ideal magnetohydrodynamics, *J. Comput. Phys.*, *154*, 284–309.

Riousset, J. A., C. S. Paty, R. J. Lillis, M. O. Fillingim, S. L. England, P. G. Withers, and J. P. M. Hale (2013), Three-dimensional multifluid modeling of atmospheric electrodynamics in Mars' dynamo region, *J. Geophys. Res. Space Physics*, *118*, 3647–3659, doi:10.1002/jgra.50328.

Schunk, R. W., and A. F. Nagy (2009), *Ionospheres,* 2nd ed., Cambridge Univ. Press, New York.

Smith, M. D. (2004), Interannual variability in TES atmospheric observations of Mars during 1999–2003, *Icarus*, *167*, 148–165.

Tóth, G., et al. (2012), Adaptive numerical algorithms in space weather modeling, *J. Comput. Phys.*, *231*, 870–903.

Valeille, A., V. Tenishev, S. W. Bougher, M. R. Combi, and A. F. Nagy (2009), Three-dimensional study of Mars upper thermosphere/ionosphere and hot oxygen corona: 1. General description and results at equinox for solar low conditions, *J. Geophys. Res.*, *114*, E11005, doi:10.1029/2009JE003388.

Verigin, M., et al. (1991), Ions of planetary origin in the Martian magnetosphere (Phobos 2/TAUS experiment), *Planet. Space Sci.*, *39*, 131–137.

Zhang, T. L., et al. (2012), Magnetic reconnection in the near Venusian magnetotail, *Science*, *336*, 567–570.